Comparison of Discharge Coefficient Measurements and Correlations for Orifices With Cross-Flow and Rotation

Marcus Hüning
Birkenhof 6,
Blankenfelde-Mahlow 15831 Germany
e-mail: marcus.huening@web.de

Gas turbines and jet engines consist of a network of connected cavities beside the main gas path called the secondary air system. These cavities, which are often surrounded by stationary and high angular speed rotating walls are exposed to varying pressure and temperature levels of air or oil contaminated air and are connected to each other by orifices or restrictors. It is vital to control the secondary flow to enable a reliable and efficient engine design, which meets component durability with a minimum of parasitic air consumption. It is essential to understand the flow physics as well as network interdependency in order to minimize the flow consumption and yet meeting engine operating requirements, as well as practical parts component design or manufacturing needs. In this connection, computer network codes containing model conceptions, which can accurately predict orifice flows, are essential. In an effort to provide usable further insight into flows across restrictors, such as orifices, this publication compares test results and orifice loss calculation models from the open literature with the aid of transformation laws and contour plots. The influence of different geometric features is incorporated into a model for the calculation of discharge coefficients. This publication is an extract of the underlying widespread and more detailed ASME paper (Huening, 2008, "Comparison of Discharge Coefficient Measurements and Correlations for Several Orifice Designs With Cross-Flow and Rotation Around Several Axes," ASME Paper No. GT2008-50976). Minor errors, noticed during adapting, are corrected. [DOI: 10.1115/1.3147102]

1 Introduction

In order to meet challenging efficiency targets, modern aircraft gas turbines are designed to operate with main gas path turbine temperatures exceeding the fatigue limit of some of the components. Therefore, colder air is bled from the compressor and distributed by the secondary air system to the challenged components, such as turbine disks, airfoils, parts of the casing, and so on. Moreover, the high pressure air from the compressor is used to seal the oil within the bearing cavities in order to isolate oil from the rest of the engine. This helps to prevent oil fires, aircraft bleed air contamination, and unacceptable oil consumption.

The air flow in the secondary air system is determined by at least one restricting loss, such as (rotating) seals between components, unpreventable leakage areas between adjacent parts, and orifices. Since the orifice geometry is generally fixed during the engine life, it is a preferred metering device because engine performance and component life are influenced by flow changes. Typically, orifices are used as stationary orifices in the static structure, radial orifices in shafts, axial orifices in turbine and compressor disks, and so on. Here, "axial" means that the orifice axis is parallel to the rotation axis of the flow relative to the orifice, and "radial" means that the orifice axis is directed in radial direction to the rotation axis.

To certify an aero-engine, the integrity of parts has to be demonstrated and life predictions have to be generated. Therefore, the orifices have to provide the required cooling flows at the critical design points taking account of worst drawing tolerances. This has to be balanced against minimum cooling flow for cruise performance. Any weakening of the surrounding material has to be minimized in order to optimize the component weight.

This publication compares orifice cross-flow correlations similar to Ref. [1], but over an extended range of geometries and based on some different and at least some more recent research results as Refs. [2,3]. After a short introduction into the theory of orifice flow, transformation laws are given to compare the different standards. The main section presents incompressible flow correlation equations from the literature for (long) radiused and chamfered orifices, which are subsequently plotted as contour plots in order to demonstrate the interaction of the independent parameters. The results are compared with the findings of other references. Two pressure ratio correction algorithms are introduced and compared with measurements by means of contour plots. Based on recent cross-flow measurements, a correlation is obtained, matched to the test data, and integrated into the calculation process. Furthermore, this test data source is compared with other cross-flow correlation. The complete process is validated with test data from an unused source.

2 Theory of (Rotating) Orifice Flow

A mass flow passing through a cross section perpendicular on the flow direction can be calculated theoretically based on a derived gas dynamic equation, the local total and static flow conditions, as well as some gas properties:

$$\dot{m} = \frac{p_t \cdot A}{\sqrt{R \cdot T_t}} \cdot \sqrt{\frac{2 \cdot \kappa}{\kappa - 1} \cdot \left[\left(\frac{p_s}{p_t} \right)^{2/\kappa} - \left(\frac{p_s}{p_t} \right)^{(\kappa+1)/\kappa} \right]} \tag{1}$$

This formula is valid for pressure ratios below the critical pressure ratio, where choking occurs:

Contributed by the International Gas Turbine Institute of ASME for publication in the JOURNAL OF TURBOMACHINERY. Manuscript received August 26, 2008; final manuscript received March 1, 2009; published online April 5, 2010. Review conducted by David Wisler. Paper presented at the ASME Turbo Expo 2008: Land, Sea, and Air (GT2008), Berlin, Germany, June 9–13, 2008.

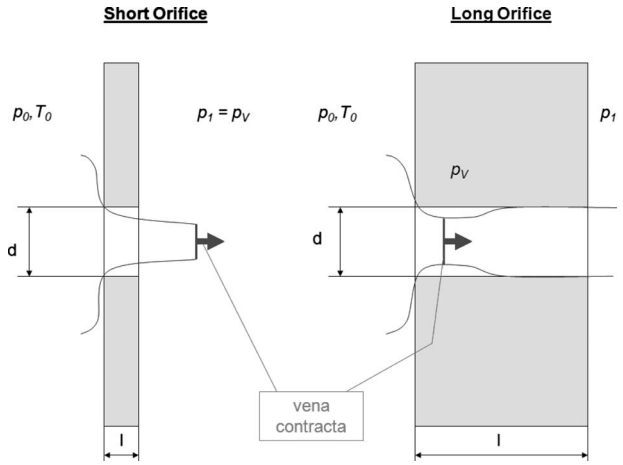

Fig. 1 Orifice flow with vena contracta

$$\frac{p_t}{p_s} \leq \left(\frac{\kappa+1}{2}\right)^{\kappa/(\kappa-1)} \tag{2}$$

This publication presents later on formulas that are valid for pressure ratios below the critical pressure ratio.

The flow through a short orifice connecting two large reservoirs can be seen as an example for the flow through a cross section. Due to the inlet separation, caused by acceleration at the entrance of the orifice, the resulting flow area is smaller than the orifice geometric area, as shown in Fig. 1 (short orifice).

Appearing total conditions in the vena contracta (flow area with parallel flow) are quite like the upstream conditions and the static pressure is similar to the downstream pressure. This motivates the definition of the discharge coefficient as the ratio of the actual mass flow divided by the theoretical mass flow through the geometrical area:

$$C_D = \frac{\dot{m}}{\dot{m}_{\mathrm{id}}} \tag{3}$$

At the vena contracta or minimum flow area, the local static pressure may not equal the discharge static pressure (Fig. 1, long orifice). Nevertheless, discharge coefficient is calculated based on upstream and downstream (discharge) conditions:

$$C_{D,\mathrm{abs}} = \frac{\dot{m}}{\frac{p_{0t}\cdot A}{\sqrt{R\cdot T_{0t}}}\cdot\sqrt{\frac{2\cdot\kappa}{\kappa-1}\cdot\left[\left(\frac{p_{1s}}{p_{0t}}\right)^{2/\kappa}-\left(\frac{p_{1s}}{p_{0t}}\right)^{(\kappa+1)/\kappa}\right]}} \tag{4}$$

Rearranged, Eq. (4) can be used to determine the mass flow for known C_D: $\dot{m}=f(p_{0t},p_{1s},T_{0t},A,C_D,\kappa)$. Correlations to determine this C_D value are presented later on in this publication.

The ideal velocity through the orifices can be calculated by the following gas dynamic equation:

$$v_{\mathrm{ax,id}} = \sqrt{\frac{2\cdot\kappa}{\kappa-1}\cdot R\cdot T_{0t}\cdot\left[1-\left(\frac{p_{1s}}{p_{0t}}\right)^{(\kappa-1)/\kappa}\right]} \tag{5}$$

Discharge coefficients C_D of orifices in real engine applications are impacted by several different aspects:

- friction (Re number, which impacts the boundary layer)
- radius or chamfer at the inlet and outlet (separation regimes and flow pattern)
- angle of axis perpendicular to inlet and exit surface (separation regimes and flow pattern)
- cross sectional shape (round, rectangular, etc.)
- length to diameter ratio (separation regimes and flow pattern)

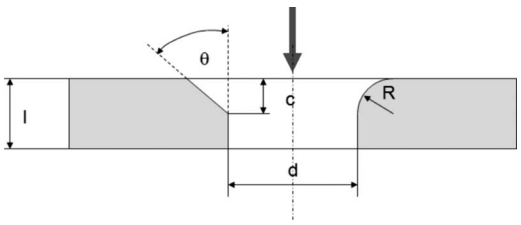

Fig. 2 Orifice geometries

- cross-flow at inlet and outlet (separation regimes and flow pattern)
- rotation by the angular speed and the position of orifice related to the axis of rotation (centrifugal and Coriolis force)
- pressure ratio (Ma number and compressibility)
- flow obstructions and changes in direction at the inlet and outlet (separation regimes, flow pattern, and turbulence)
- disturbance of inlet flow (other orifices, disk pumping boundary layer development, turbulence, and so on)

The impact of these items on the orifice discharge behavior has been analyzed by different experiments and by various authors over the past years. Moreover, continuous research is performed to clear out open issues and contradictions in understanding.

A sophisticated separation of C_D is used inter alia by Dong and Lienhard [4]:

$$C_D = C_V \cdot C_C \tag{6}$$

In industrial flow measurement, pressure taps measure the static pressure upstream and downstream of orifices [5] and analyzes the error, which appears for small reservoirs and provides further references.

Figure 2 shows at least some geometric dimensions, which impact the discharge coefficient of orifices.

Cross-flow at the orifice inlet leads generally to two dedicated phenomena, as follows.

- An increased separation regime on the side of the upstream flow, which reduces the effective flow area and, therefore, tends to decrease the orifice through flow.
- A flow stagnation in the relative system against the relative direction of the attacking flow, perpendicular to the orifice axis subsequently after entering the orifice, which leads to a (partly) recovering of the relative dynamic head of the cross-flow. Therefore, the flow is driven by a pressure between the total and the relative total pressure through the vena contracta, which tends to increase the orifice through flow.

The relative total conditions can be calculated from Eqs. (7) and (8) based on the total conditions:

$$T_{0t,\mathrm{rel}} = T_{0t}\cdot\left(1+\frac{u^2}{2\cdot c_P\cdot T_{0t}}\right) \tag{7}$$

$$p_{0t,\mathrm{rel}} = p_{0t}\cdot\left(1+\frac{u^2}{2\cdot c_P\cdot T_{0t}}\right)^{\kappa/(\kappa-1)} \tag{8}$$

Hereby the circumferential velocity u can be understood more generally as the relative velocity perpendicular to the surface normal vector, which is later on explained in Eqs. (17) and (18). This requires that the total conditions are measured in a reference frame, which is rotating with the upstream flow.

Hence Eqs. (7) and (8) account for the rotational work transfer and the change in the reference system [6] or to put it more simple the impact of flow stagnation in the relative system.

The phenomenon of the relative flow stagnation motivates the definition of a discharge coefficient in analogy with Eq. (3), which uses the relative total conditions:

$$C_{D,\mathrm{rel}} = \frac{\dot{m}}{\frac{p_{0t,\mathrm{rel}} \cdot A}{\sqrt{R \cdot T_{0t,\mathrm{rel}}}} \cdot \sqrt{\frac{2 \cdot \kappa}{\kappa - 1} \cdot \left[\left(\frac{p_{1s}}{p_{0t,\mathrm{rel}}} \right)^{2/\kappa} - \left(\frac{p_{1s}}{p_{0t,\mathrm{rel}}} \right)^{(\kappa+1)/\kappa} \right]}} \tag{9}$$

This definition is easier to understand for rotating inlet flow and additional rotating orifices. Moreover, this formulation leads to C_D values strictly between 0 and 1, which is more stable for correlating Refs. [1,2]. Therefore, all discharge coefficients describing cross-flow are presented in the relative C_D formulation. For cases without cross-flow, Eqs. (9) and (4) lead to the same results.

The ideal velocity in the relative frame of reference through the orifices can be calculated by the following equation:

$$w_{\mathrm{ax,id}} = \sqrt{\frac{2 \cdot \kappa}{\kappa - 1} \cdot R \cdot T_{0t,\mathrm{rel}} \cdot \left[1 - \left(\frac{p_{1s}}{p_{0t,\mathrm{rel}}} \right)^{(\kappa-1)/\kappa} \right]} \tag{10}$$

Rotation of the orifices or the flow goes along with two additional forces, which are acting on the flow: the centrifugal and the Coriolis force [7].

The pumping flow in radial direction in the vicinity of a rotating disk due to acting centrifugal force can be approximated by the following free disk equation [8]:

$$\dot{m} = 0.219 \cdot \mu \cdot r_m \cdot \mathrm{Re}_{\Phi}{}^{0.8} \tag{11}$$

This pumped flow has a radial and a circumferential component [9], which shows experimental results of Erian and Tong (1971), proving the circumferential velocity about five times higher than the radial velocity. The circumferential velocity drops from disk speed to a fraction of about 0.4 down to about 0.2 in the area where the pumping flow is located. One fraction of the pumped flow mixes with the orifice flow. Its circumferential component reduces the incidence angle, and the radial component increases it. This publication determines the order of the pumping flow and compares it with a determined orifice flow for the later on correlated results of Ref. [2].

3 Transformation Laws for (Rotating) Orifices With Cross-Flow

The impact of cross-flow and rotation on the discharge coefficient of orifices has been analyzed by several different experiments and authors over the last years using different notations. The succeeding formulas give a set of transformation laws in order to compare the different measurements.

There are two basic definitions of the discharge coefficient C_D, one using the total upstream pressure and temperature for nonrotating inlet flow $C_{D,\mathrm{abs}}$ and the other one using the relative total pressure and temperature with the orifice inlet as a reference system $C_{D,\mathrm{rel}}$. The following equation provides a transformation law between both definitions, which can be deduced by division of its upfront given definitions:

$$\frac{C_{D,\mathrm{rel}}}{C_{D,\mathrm{abs}}} = \frac{\dot{m}_{\mathrm{id,abs}}}{\dot{m}_{\mathrm{id,rel}}} = \frac{v_{\mathrm{ax,id}}}{w_{\mathrm{ax,id}}} = \sqrt{1 - \frac{u^2}{w_{\mathrm{ax,id}}^2}} = 1/\sqrt{1 + \frac{u^2}{v_{\mathrm{ax,id}}^2}} \tag{12}$$

The amount of cross-flow is described by at least four different notations in the studied literature:

1. $u/v_{\mathrm{ax,id}}$: absolute velocity ratio
2. $u/w_{\mathrm{ax,id}}$: relative velocity ratio
3. i: incidence angle
4. Θ_v: velocity head ratio

The definition of the first two notations is obvious. The incidence angle 3. is defined by the following equation [3,10]:

$$i = \arctan(u/w_{\mathrm{ax,id}}) \tag{13}$$

The velocity head ratio is defined as:

$$\Theta_v = \frac{p_{0t,\mathrm{rel}} - p_{1s}}{p_{0t,\mathrm{rel}} - p_{0s}} \tag{14}$$

This work uses the notation of the incidence angle i to present the data to enable an easy imagination. To understand the transformed results from other authors, the transformation laws for the different notations describing the cross-flow effect are summarized.

The parameters, which are used in the first two notations, are linked by the following transformation law, which can be deduced by the definition equations and the definition of the relative total conditions upfront:

$$w_{\mathrm{ax,id}} = \sqrt{u^2 + v_{\mathrm{ax,id}}{}^2} \tag{15}$$

This is the geometric structure of a rectangular velocity triangle. Rearrangement for the notations used:

$$\frac{u}{w_{\mathrm{ax,id}}} = 1/\sqrt{1 + 1/\left(\frac{u}{v_{\mathrm{ax,id}}} \right)^2} \tag{16}$$

A definition of a relative cross-flow velocity combining the effect of rotation, swirl, and passing flow or disk pumping is given by Eq. (17):

$$c_{0,\mathrm{rel}} = \sqrt{u^2 + c_{\perp u}^2} \tag{17}$$

In most cases an easier expression is valid, but in some cases a replacement in the former equations of u with $c_{0,\mathrm{rel}}$ can improve the accuracy of the calculation:

$$c_{0,\mathrm{rel}} = u \tag{18}$$

In Ref. [10], a transformation between notations 2 and 4 is deduced. This transformation is improved in this publication to be valid even for higher pressure ratios below the critical pressure ratio:

$$\frac{c_{0,\mathrm{rel}}}{w_{\mathrm{ax,id}}} = \sqrt{\frac{1 - \left(\frac{p_{0s}}{p_{0t,\mathrm{rel}}} \right)^{(\kappa-1)/\kappa}}{1 - \left(\frac{p_{1s}}{p_{0t,\mathrm{rel}}} \right)^{(\kappa-1)/\kappa}}} = \sqrt{\frac{1 - 1/\left(1 + \frac{\kappa - 1}{2} \cdot \mathrm{Ma}_{\mathrm{rel}}{}^2 \right)}{1 - \left(1 - \Theta_v \cdot \left\langle 1 - 1/\left(1 + \frac{\kappa - 1}{2} \cdot \mathrm{Ma}_{\mathrm{rel}}{}^2 \right)^{\kappa/(\kappa-1)} \right\rangle \right)^{(\kappa-1)/\kappa}}} \tag{19}$$

This transformation is dependent on the velocity head ratio and the relative Mach number upstream of the orifices. The static pressure ratio can be calculated using the following equation:

$$\frac{p_{1s}}{p_{0s}} = \left(1 + \frac{\kappa - 1}{2} \cdot \mathrm{Ma}_{\mathrm{rel}}{}^2 \right)^{\kappa/(\kappa-1)} \cdot (1 - \Theta_v) + \Theta_v \tag{20}$$

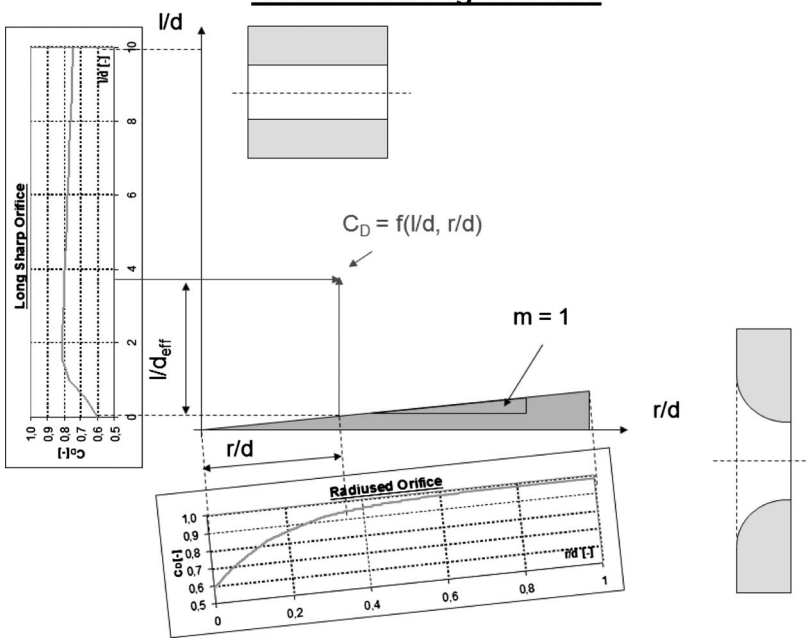

Fig. 3 C_D **of radiused (long) orifices**

4 Discharge Coefficient Correlations, Measurements, and Integration Into One Calculation Process

There are two dedicated methods to correlate discharge coefficients for computer applications.

1. Plotting measured data and performing an empirical curve fit by finding describing mathematical expressions, most suitable for scaling factors in between a physical maximum and a minimum of the correlated parameter.
2. Developing a real physical model conception of the physics of the flow and adjusting it with matching factors to measured test data.

The literature, which was studied in order to write this publication, provides examples for both types but is dominated by the first type, which will also be applied as the principal proceeding in this publication. Examples for the second type are Ref. [11], in which the author develops a compressibility correction for orifices and convergent nozzles based on an assumption of flow distribution, and Ref. [12] where assumptions of velocity profiles are made to describe the separated losses in rotating passages.

Discharge coefficient correlations from the first type, which are analyzed for this publication, are based on or are at least similar to the approach of McGreehan and Schotsch [13] and enlarged the applicability or improve its accuracy. Recent work on this field is published by Idris, Pullen and co-workers [3,14].

4.1 Reynolds Number. The first step to determine discharge coefficients is to calculate Reynolds number corrected incompressible basis discharge coefficients, which are subsequently used as a threshold for the correlated discharge coefficients. For this purpose, a sharp orifice (Eq. (21)) and a nozzle (Eq. (22)) are correlated:

$$C_{D,\text{sharp orifice}} = 0.5885 + \frac{372}{\text{Re}_{ax}} \tag{21}$$

$$C_{D,\text{nozzle}} = 0.9981 - \frac{4.73}{\sqrt{\text{Re}_{ax}}} \tag{22}$$

Both equations are presented by McGreehan and Schotsch [13] and are valid for $\text{Re}_{ax} > 10{,}000$. The overall impact of the Reynolds number is for high Reynolds numbers, as appeared in secondary air systems of aero-engine applications, from the second order effect [15,16].

4.2 Inlet Radiusing and Chamfering. The second step is either an inlet radius correction or an inlet chamfer correction of the basis incompressible C_D values. Hay and Spencer [17] stated that the increase in C_D with increasing r/d occurs because the local acceleration of the fluid around the periphery drops and separation becomes less likely. The following inlet radius correction was originally presented by McGreehan and Schotsch [13] but was improved by Parker and Kercher [5] to avoid unphysical discharge coefficient predictions for nonrotating orifices of up to one (Class 1 orifice):

$$C_{D,\text{radius}} = C_{D,\text{nozzle}} - f \cdot (C_{D,\text{nozzle}} - C_{D,\text{sharp orifice}}) \tag{23}$$

$$f = 0.008 + 0.992 \times e^{-5.5(r/d)-3.5(r/d)^2} \tag{24}$$

Inlet chamfered orifices are correlated by Idris and Pullen [3] to the data of Hay and Spencer [17]. The following expressions are published:

$$C_{D,\text{chamfer}} = 1 - h \cdot (1 - C_{D,\text{sharp orifice}}) \tag{25}$$

$$h = \left[1 - \left\{ \begin{matrix} (1 - e^{-25.3(c/d)}) \\ \langle((26.16 + \theta)/(43.63 + 0.0184 \cdot \theta^2)) - 0.6\rangle + 0.6 \end{matrix} \right\} \right] / 0.4 \tag{26}$$

4.3 Axial Length. The axial length impacts the re-attachment ability of the separated orifice flow and thereby the dynamic head recovery. So the third step is a correction of axial length based on the equations presented by McGreehan and Schotsch [13] (Class 2 orifice):

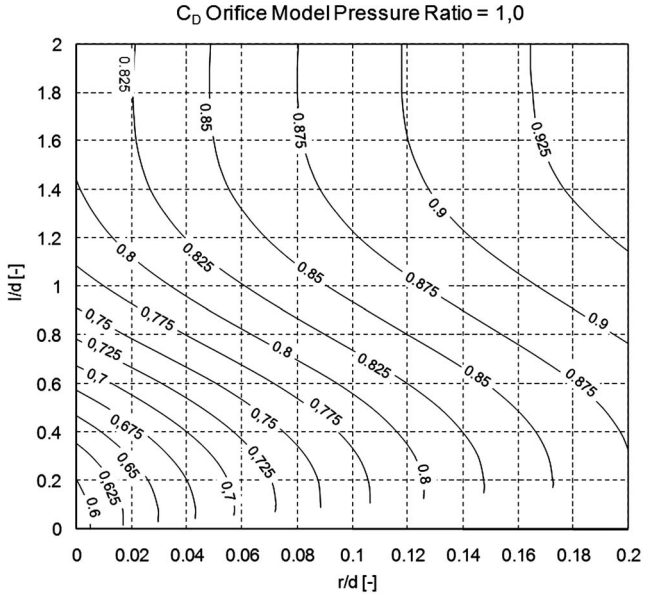

Fig. 4 C_D **of incompressible (long) orifices with inlet radius**

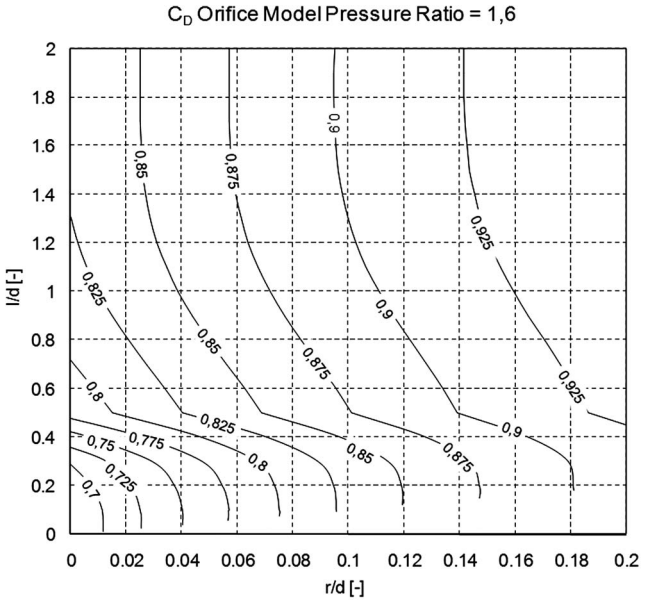

Fig. 5 C_D **of correlated (long) orifices with inlet radius for a pressure ratio of 1.6**

$$C_{D,\text{long orifice}} = 1 - g \cdot (1 - C_{D,\text{sharp orifice}}) \tag{27}$$

$$g = [1 + 1.3 \times e^{-1.606\cdot(l/d)^2}] \cdot \left(0.435 + 0.021 \cdot \frac{l}{d}\right) \tag{28}$$

Figure 3 illustrates the procedure for additional accounting of inlet radiusing for long orifices (Class 3 orifice). Chamfered orifices are treated in the same way as radiused ones. For the calculation of radiused or chamfered long orifices the $C_{D,\text{sharp orifice}}$ (27) is substituted by the respective C_D value for radius (23) or chamfer impact (25). Furthermore, the length is substituted by an effective length, which is reduced by the inlet radius, or in the same way by the inlet chamfer depth, in Eqs. (27) and (28). This leads to the equations:

$$C_{D,\text{long orifice}} = 1 - g \cdot (1 - C_{D,\text{radius}}) \tag{29}$$

$$g = [1 + 1.3 \times e^{-1.606\cdot((l-r)/d)^2}] \cdot \left(0.435 + 0.021 \cdot \frac{l-r}{d}\right) \tag{30}$$

Equations (29) and (30) are presented similar to Ref. [5] due to the fact that an additional accounting of the radius or chamfer effect as proposed by McGreehan and Schotsch [13] and Idris and Pullen [3] has minor impact on the result. Moreover, the version presented by Parker and Kercher [5] is more traceable.

4.3.1 Visualization of Incompressible Correlations. The so correlated incompressible discharge coefficients for long radiused orifices lead to the contour plots shown in Fig. 4, assuming a sufficient high Reynolds number. Figure 4 reflects the statement of Hay and Spencer [17] that inlet radiusing has a more significant effect on the discharge coefficient of short orifices. Hay and Spencer [17] summarized the effect of chamfering and radiusing to cause the plateau of maximum C_D to start at a lower l/d.

4.4 Pressure Ratio Correction. In real engine applications, as well as for published research test results, pressure ratios significantly higher than order unity appear. Therefore, a compressibility correction is necessary to transfer all data on a common basis for C_D comparison. In the earlier publications like Ref. [13], this was performed by the implementation of an adiabatic expansion factor Y into an incompressible mass flow equation. Hence, the compressibility effects are not ascribed to the C_D value, but are instead incorporated into the calculation procedure subsequently to cross-flow effects. Bragg [11] developed an analytical compressibility correction for orifices and convergent nozzles based on an assumption of upstream flow distribution, which is applicable to Class 1 orifices but overpredicts the effect of pressure ratio for long orifices (Class 2 and Class 3) [16]. Bragg [11] and Hay and Spencer [17] stated that increasing pressure ratio increases C_D, especially for short orifices due to an expansion of the vena contracta. Idris and Pullen [3] presented a pressure ratio correction only based on an incompressible C_D value and the pressure ratio. It is noted that this approach is not able to cover dedicated l/d and r/d effects similar to Ref. [11]. Parker and Kercher [5] presented an empirical curve fit, which links the incompressible C_D*s* without cross-flow based on equations similar to these used by McGreehan and Schotsch [13] and shown in Eqs. (23), (24), (29), and (30) with compressible test data inter alia from Ref. [16], with the intermediate step of an adiabatic expansion factor Y. This approach is only presented by Parker and Kercher [5] for rounded but not for chamfered inlets and covers the full range of pressure ratios. It is restricted to length to diameter ratios up to 2, but can be extended by a Fanno friction approach. It only calculates average values for the pressure hysteresis observed by Deckker and Chang [16], which is caused by the flow reattachment behavior. Due to the "easiness" of programming and its broad applicable range, it is used in this publication to calculate a static compressible C_D, which is subsequently cross-flow corrected. Hay and Spencer [17] stated that the impact of pressure ratio for nonsharp edged short orifices is small for pressure ratios above 2, which is in line with Ref. [16] and the used approach from Ref. [5].

The so correlated data are shown in Fig. 5 for a pressure ratio of 1.6. A comparison with Fig. 4 shows the impact of the compressibility correction. The C_D*s* of a sharp edged short orifice are increased from the order of 0.6 to 0.7. The l/d ratio for the same discharge coefficient is reduced for orifices with l/d ratios above 0.4 in superposition with a decrease in the needed r/d ratio.

Hay and Spencer [17] presented discharge coefficients measurements for stationary orifices for several l/d ratios in between 0 and 2, with radiused and chamfered (30 deg and 45 deg) inlets with a respective ratio up to 0.2. The data were measured for pressure ratios in between 1.2 and 2.2 with a test orifice diameter of 10 mm and a flow meter according to British Standard Speci-

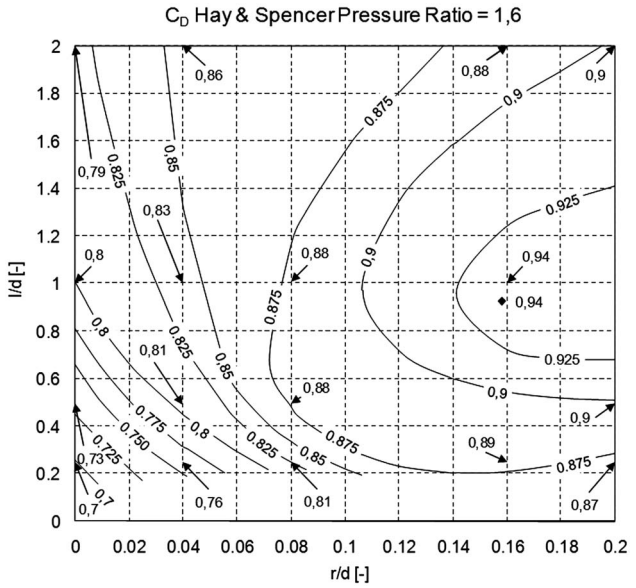

Fig. 6 C_D **of (long) orifices with inlet radius for a pressure ratio of 1.6 derived from Ref. [17]**

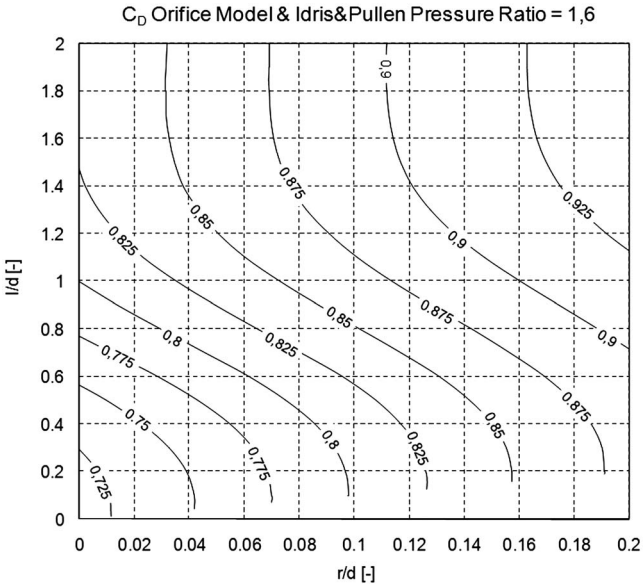

Fig. 8 C_D **of correlated (long) orifices with inlet radius for a pressure ratio of 1.6 using [3]**

fication 1042. Comparison with other authors [16] (sharp orifices) shows a C_D uncertainty of $\pm 5\%$. The geometry was checked for burs and dimensions.

Figure 6 shows the contour plot of test results published by Hay and Spencer [17] for inlet radiused orifices at a pressure ratio of 1.6 in order to validate the so correlated discharge coefficients. The arrows mark the measured geometries with their values. A comparison for the measured geometries of Ref. [17] with the correlated values (Fig. 5) shows a maximum error of 7.4% for $r/d=0$ and $l/d=0.5$ and an average error of about 2.5%. This supersedes the quoted uncertainty by Hay and Spencer [17] of about 5%. A comparison between Figs. 5 and 6 for the measured geometries used later on to correlate cross-flow effects (Fig. 7) shows differences between measurements and the correlation up to 3.3% (especially 3.1% with $r/d=0.10$ for the shorter orifices of $l/d=0.4$ and 1.3% for the longer orifices of $l/d=1.25$ with $r/d=0.05$). This is inside of the quoted uncertainty band by Hay and Spencer [17] of about 5%. The characteristics of the iso (constant level) C_D lines show two differences: the direction of bending for $l/d<0.4$ and the continuation for high l/d and r/d ratios. Based on the given accuracy all of them are potentially describing the behavior of the flow.

Furthermore, Fig. 8 shows the correlated discharge coefficients with a pressure ratio correction based on Ref. [3] applied on the whole plotted range. A comparison between Figs. 8 and 6 for the measurement positions of Ref. [17] shows the highest errors of this pressure correction at l/d ratios of about 0.5. The deviation is here for a ratio of $r/d=0.08$ about 8.6%. The average deviation for the measured geometries [17] is 3%. It is important to mention that this is the only tested approach, which can be calculated with a simple scientific calculator.

The best conformance with the measurements plotted in Fig. 6 is shown in Fig. 5 for the whole range. The method by Parker and Kercher [5] is therefore subsequently applied.

4.5 Cross-Flow Effect. There are several different studies published in literature showing measured discharge coefficients for cross-flow and rotation over a wide range of geometries, rotational arrangements, pressure ratios, and Reynolds numbers. Gen-

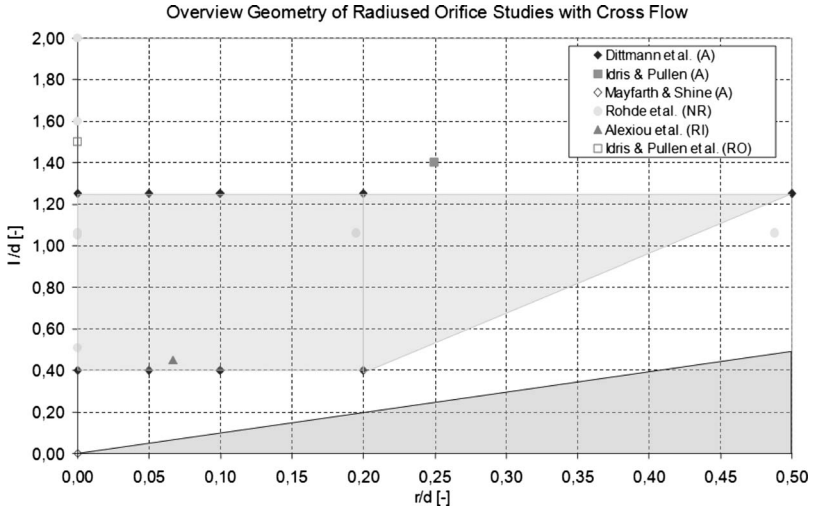

Fig. 7 Overview about geometries of radiused orifice studies with cross-flow

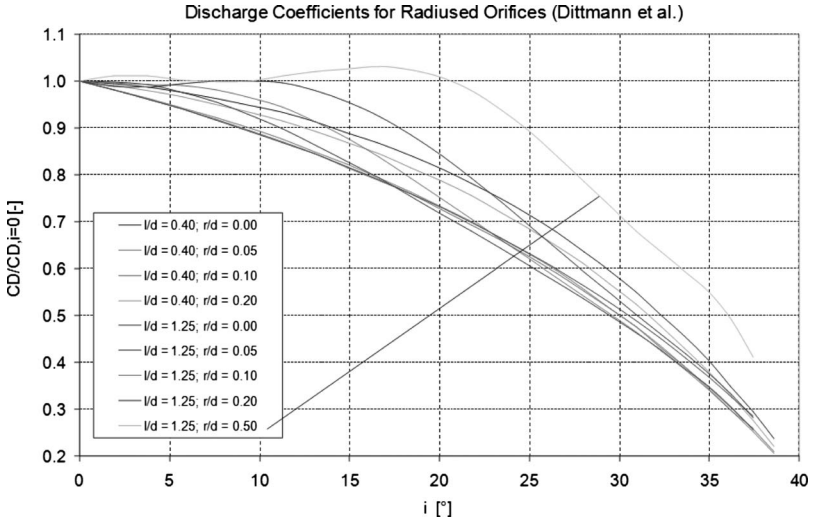

Fig. 9 $C_D/C_{D,i=0}$ **for radiused orifices from Ref. [2]**

erally, the effect of cross-flow leads to a decrease in the discharge coefficient due to an increased separation regime at the upstream edge of the orifice, which decreases the vena contracta flow area. The geometry is judged to have a significant impact on the discharge coefficient even for cross-flow. Therefore, Fig. 7 provides a visual impression about some of the tested geometries with radiused orifice inlets. The mentioned measurements (Fig. 7) are published by Dittmann et al. [2], Idris and Pullen [3], Meyfarth and Shine [18], Rohde et al. [19], and Idris et al. [10]. The abbreviations mean: A for axial, NR for no rotation, RI for radial inwards, and RO for radial outwards.

This publication presents correlated cross-flow effects for orifices with inlet radiusing based on published measurements by Dittmann et al. [2], due to the presented consistent data from one test facility for two interesting l/d ratios (smaller two) and several inlet radius (and chamfer) geometries, which cover a range of geometries as marked in Fig. 7.

The experimental setup used by Dittmann et al. [2] consisted of a rotating disk with four axial directed orifices on a mean radius of $r_m=105$ mm with a diameter of 15 mm each. The disk rotated up to 9500 1/min, which is equivalent with a Reynolds number of $\mathrm{Re}_\Phi=8.6\times10^5$. The parasitic leakage flow between the rotating and static parts, in parallel to the orifice flow, was determined by calibration measurements. The mass flow rates were determined by use of an orifice metering system in accordance to European standard with an accuracy of $\pm1\%$. The tested pressure ratios were between $\pi=1.05$ and $\pi=1.60$. Due to the speed limitations of the rotor, the maximum cross-flow test points are only reached with the lower pressure ratios.

The statement by Dittmann et al. [2] that the discharge coefficient is independent from the pressure ratio, which is shown for long orifices with the maximum tested inlet radius, is judged to be not universally valid, especially for stationary orifices (comparison with Ref. [5]). Hence the presented curves are understood as an average of the tested pressure ratios of 1.05, 1.10, 1.30, 1.50, and 1.60 for small relative cross-flow speeds and only the smaller pressure ratios for higher cross-flow speeds.

As stated above the effect of disk boundary layer pumping is estimated based on Eq. (11) at the critical case of low orifice through flow and maximum rotational speed. The disk boundary layer pumping flow is determined to be 0.0224 kg/s ($\mathrm{Re}_\Phi=8.6\times10^5$ and $\mu=17.4\times10^{-6}$ kg/m s). The calculated orifice flow is about 0.078 kg/s for this critical case so the pumping flow is about 30% of the orifice through flow and may impact the determined C_D by its reduced cross-flow speed. Nevertheless, the impact of the disk boundary layer pumping is disregarded in the presented correlation, due to the small orifice diameter of 4×15 mm compared with the circumference, related to the mean radius of 105 mm.

To combine the measured cross-flow effects of Ref. [2] with the former calculated pressure corrected [5] discharge coefficients both are compared in Table 1 especially for a pressure ratio of 1.3. This comparison shows differences of up to 9.5% with $r/d=0.10$ for the shorter orifices of $l/d=0.4$ and 4.1% for the longer orifices of $l/d=1.25$ with $r/d=0.05$. The red marked numbers in Table 1 are not inside the band of the orifice model.

To join the discharge coefficients, even with the discrepancies for the cases without cross-flow, the data for radiused orifices published by Dittmann et al. [2] are plotted as $C_D/C_{D,i=0}$ versus incidence angle i.

These curves are subsequently correlated by the following formula, which is judged to be applicable to match the test data:

Table 1 Comparison between orifice model and Ref. [2]

Dittman et al. Radiused Holes: i = 0°									
r/d	0,00	0,00	0,05	0,05	0,10	0,10	0,20	0,20	0,50
l/d	0,40	1,25	0,40	1,25	0,40	1,25	0,40	1,25	1,25
CD	**0,680**	**0,786**	**0,825**	**0,888**	**0,897**	**0,923**	**0,948**	**0,955**	**0,955**
Pressure Ratio	Orifice Model								
1,05	0,641	0,792	0,720	0,839	0,786	0,877	0,880	0,931	0,986
1,10	0,651	0,795	0,728	0,842	0,792	0,880	0,884	0,932	0,987
1,30	**0,691**	**0,809**	**0,761**	**0,853**	**0,819**	**0,889**	**0,899**	**0,938**	**0,989**
1,50	0,725	0,819	0,790	0,862	0,842	0,896	0,913	0,943	0,991
1,60	0,741	0,824	0,803	0,866	0,853	0,899	0,919	0,945	0,992
Average	**0,690**	**0,808**	**0,761**	**0,852**	**0,818**	**0,888**	**0,899**	**0,938**	**0,989**

Table 2 Coefficients for correlated radiused orifices

l/d	r/d	0,00		0,05		0,10		0,20		0,50	
0,40	b1	3,8818E+01	b1	2,0072E+09	b1	8,9051E+02	b1	1,0719E+02			
	b2	7,1443E-05	b2	-4,7070E+08	b2	4,9939E+08	b2	1,1045E-04			
	b3	1,2651E+00	b3	3,6469E+07	b3	4,2256E+07	b3	2,0305E+00			
	b4	2,6770E+01	b4	3,5034E+01	b4	3,6941E+01	b4	2,8734E+01			
	b5	6,8889E-01	b5	1,0875E+00	b5	1,1789E+00	b5	7,7599E-01			
	b6	2,0178E+01	b6	2,0675E+01	b6	2,1371E+01	b6	1,8456E+01			
	b7	3,3953E-01	b7	1,1561E+00	b7	1,1793E+00	b7	7,8828E-01			
1,25	b1	-1,0055E+03	b1	2,2400E+00	b1	1,0810E+01	b1	1,4849E+01	b1	1,9919E+01	
	b2	-6,8224E+09	b2	5,4180E-03	b2	5,7169E-02	b2	3,4088E-02	b2	9,5706E-02	
	b3	2,4775E+09	b3	2,3623E+00	b3	7,0397E+00	b3	4,7473E+00	b3	6,3318E+00	
	b4	4,0177E+01	b4	2,1655E+01	b4	3,7874E+01	b4	3,5175E+01	b4	2,4293E+01	
	b5	1,2056E+00	b5	3,3143E-01	b5	1,9351E+00	b5	2,5651E+00	b5	-6,8695E-01	
	b6	1,9866E+01	b6	3,6611E+01	b6	5,9657E+01	b6	1,5288E+02	b6	4,0709E+00	
	b7	1,2026E+00	b7	5,9411E-01	b7	1,1517E+00	b7	1,1366E+00	b7	8,9253E-01	

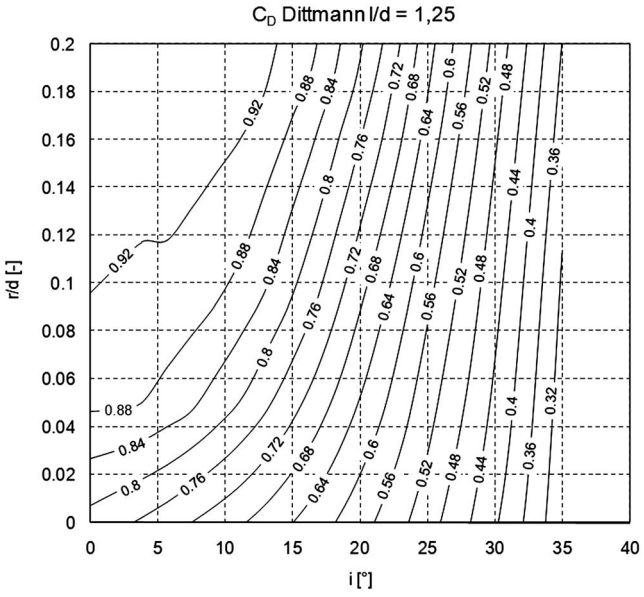

Fig. 10 Impact of incidence angle on discharge coefficient based on Ref. [2] for *l*/*d*=1.25

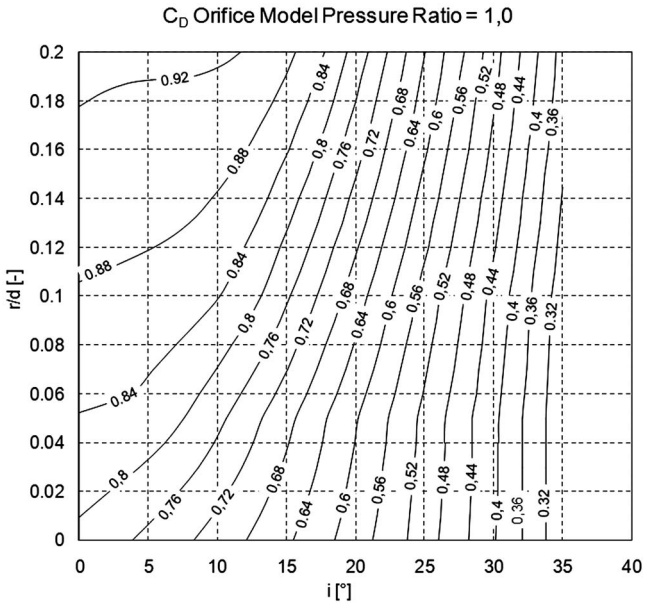

Fig. 11 Impact of incidence angle on discharge coefficient with determined correlation for *l*/*d*=1.25

$$C_D/C_{D,i=0} = \frac{1}{(i-b_1)^2 \cdot b_2 + b_3} - \frac{e^{(i/b_4+b_5)}}{b_6} \cdot (i/b_4 + b_5) + b_7 \quad (31)$$

Formula (31) is particularly designed to model the plateau in some of the plots. The formula should be applicable for chamfered orifices as well.

The determined coefficients are summarized in Table 2. The presented curve fits match the presented plots of Fig. 9 within ±2.8% accuracy for incidence angles below 35 deg. The average accuracy for the complete data is 0.43%.

It is proposed to determine data points in between the correlated geometries by linear interpolation for the r/d and l/d ratio.

For a fast and preliminary design, the following formula matches the data shown in Fig. 9 for $r/d <= 0.2$ with an accuracy of ±13.29%:

$$C_D/C_{D,i=0} = -4.4513 \times 10^{-4} \cdot i^2 - 2.9937 \times 10^{-3} \cdot i + 1 \quad (32)$$

As shown in Fig. 8 the data of Ref. [18], one of the earliest studies, can potentially be applied to extend the range of supporting points for the correlation for short and sharp orifices, due to the small C_D*s* for stationary orifices. Both plots show plateaus as well, which are seen in Ref. [2] only for longer orifices with nonsharp edged inlets.

The following plots, prepared to compare the impact of cross-flow, are created for the theoretical pressure ratio of 1 (incompressible flow). Nevertheless, the data in Fig. 10 are plotted as presented by Dittmann et al. [2] (no pressure ratio correction). The stationary C_D is calculated for all other plots by the proposed approach.

Figure 10 shows a contour plot of discharge coefficients derived from Ref. [2] transformed versus the incidence angle. The instabilities for low incidence angles are judged to depend on the wavy measurements, as seen in Fig. 9.

Figure 11 shows a contour plot of the correlated discharge coefficients versus the incidence angle. Figures 10 and 11 show a similar characteristic of the iso discharge coefficient lines. The average accuracy in a direct comparison is 3.94%. The maximum error is 6.4%. These errors are significantly impacted by the error shown in Table 1.

Figure 12 shows a contour plot of discharge coefficients derived from Ref. [13] transformed versus the incidence angle and to relative total discharge coefficients $C_{D,\mathrm{rel}}$. Figure 12 shows an increase in the discharge coefficient with the incidence angle for all radii for incidence angles smaller than about 6 deg. For higher incidence angles, a decrease is shown. The average accuracy in a direct comparison with Fig. 10 is 24.43%. The maximum overprediction is 90% observed for $r/d=0.1$ and a maximum incidence angle of 35 deg. The maximum absolute error appears for $r/d=0.16$ and a maximum incidence angle.

Rohde et al. [19] presented discharge coefficients for cross-flow based on a main channel with 0.25 in. (6.3 mm) diameter and one orifice at the side of the channel. Orifice geometries inter alia shown in Fig. 7 were tested. It is stated that the orifice geometries were carefully examined and measured with optical instruments and plug gauges. Figure 13 shows some of the test results for inlet

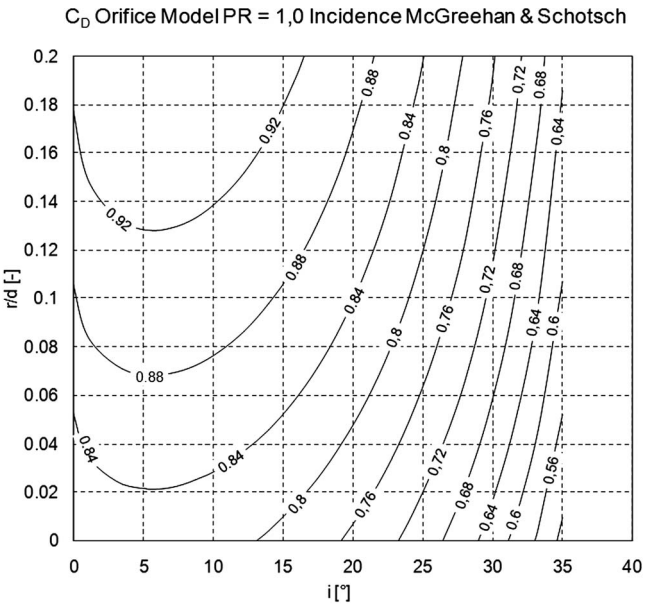

Fig. 12 Impact of incidence angle on discharge coefficient based on Ref. [13] for *l*/*d*=1.25

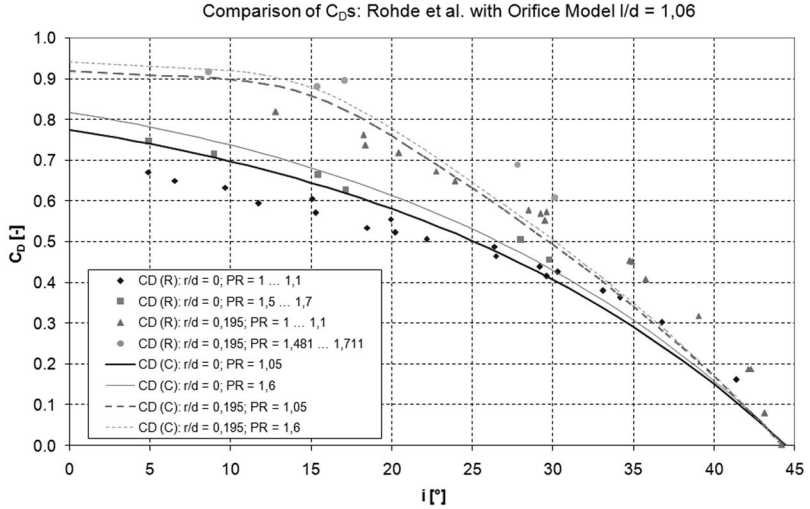

Fig. 13 Comparison of discharge coefficient based on Ref. [19] with the determined correlation

radiused orifices with r/d ratios of 0 and 0.195 for two ranges of pressure ratio centered at 1.05 and at 1.6. The abbreviations mean R for Rohde and C for correlation. The determined correlation matches the data from Ref. [19] quite well with respect to the uncertainties of former comparisons of test data with other correlations. The maximum error of 32.0% between the correlation and an equalized curve of the test data appear for $r/d=0.195$ and the pressure ratio of 1.05 (from $i=0$ deg to $i=35$ deg). The transformed test data show a higher impact of the pressure ratio on the discharge coefficient, especially for the inlet radiused orifice, than correlated by Parker and Kercher [5]. The correlation (stationary orifice) tends to overpredict the sharp edged orifice discharge coefficients for incidence angles up to 25 deg. The data of Ref. [2], which were used to generate the cross-flow correction, are in this range about 2.7% lower than these of the stationary orifice model. Moreover, the correlation tends to underpredict the flow for incidence angles above 30 deg, which leads to the maximum error mentioned above. This phenomenon is potentially increased by disregarding the pressure ratio effect, which is not quoted in the results of Ref. [2].

An improvement of the cross-flow correlation, which is joined to the orifice model, especially for small l/d ratios, is potentially possible by the following assumption: The C_Ds of Ref. [2] for a given amount of cross-flow are averages for the different pressure ratios, as given in Fig. 6 of Ref. [2], for all tested geometries. This requires to correct the presented results with the data based on Table 1 upfront a new curve fit.

5 Summary and Conclusions

The presented publication starts with an introduction into the theory of (rotating) orifice flow (with cross-flow) and provides two common definitions of discharge coefficients C_D. Several items, especially geometric parameters, which impact these C_D values are summarized. Furthermore, transformation laws are presented to exchange the two presented definitions of the C_D value and transform commonly published parameters describing cross-flow into each other. A calculation process for incompressible static orifice flow is summarized from different sources. Two pressure correction algorithms are compared with measurements [17]. An algorithm based on Ref. [5] is subsequently applied. The impact of boundary layer pumping for a rotating disk, which is subsequently used for correlating, is demonstrated by a hand calculation with low orifice through flow rates and is judged to be minor. The impact of cross-flow on inlet radiused orifices is correlated for a wide range of test data based on Ref. [2] and compared with other correlations and independent test results of Ref. [19]. Thereby significant uncertainties compared with the test data appear for the foreign correlation at high incidence angles up to 35 deg. The correlation presented here matches both test data sources relatively well.

Due to the relatively high differences between discharge coefficients from different sources, the importance of exact manufactured orifice geometries and subsequent inspections for burs and dimensions was noticed. Moreover, it was noticed that different experimenters measured the flow according to different standards.

Acknowledgment

The author would like to thank all the people who helped find or get the literature used herein and provided revision proposals for the phrasing of this text.

Nomenclature

A = cross-sectional area (m^2)
b = constant in formulas
c = chamfer depth at the orifice inlet corner (mm)
$c_{\perp u}$ = velocity perpendicular u parallel to the surface wall (m/s)
$c_{0,\mathrm{rel}}$ = velocity at the inlet, relative to the orifices and parallel to the surface wall (m/s)
C_C = contraction coefficient (jet area/orifice area)
C_D = discharge coefficient (actual mass flow/ideal mass flow)
C_V = velocity coefficient (jet velocity/ideal jet velocity)
c_P = specific heat capacity (J/kg K)
d = diameter (mm)
f = scaling factor (r/d correlation)
g = scaling factor (l/d correlation)
h = scaling factor (c/d correlation)
i = incidence angle (deg)
l = length (mm)
m = slope
$\dot{m}$ = mass flow rate (kg/s)
Ma = Mach number
n = rotational speed (1/min)
p = pressure (kPa)
r = radius at inlet corner (mm)
r_m = pitch radius of the orifices (mm)
R = specific gas constant (J/kg K)

Re_{ax} = axial Reynolds number ($\mathrm{Re}_{ax}=\dot{m}\cdot d/(A\cdot\mu)$)
Re_{Φ} = rotational Reynolds number ($\mathrm{Re}_{\Phi}=\omega\cdot r_m^2/\nu$)
T = temperature (K)
u = circumferential velocity relative to the orifices (m/s)
v_{ax} = velocity axial through the orifices in the absolute frame of reference (without relative stagnation effect) (m/s)
w_{ax} = velocity axial through the orifices in the relative frame of reference (m/s)
Y = adiabatic expansion factor
κ = isentropic exponent
μ = dynamic viscosity (kg/m s)
ν = kinematic viscosity m^2/s
π = total pressure ratio ($\pi=p_{0t}/p_{1s}$)
Θ = velocity head ratio
θ = chamfer angle at the orifice inlet corner (deg)
ρ = density (kg/m^3)
ω = angular velocity of the rotor (1 s)

Subscripts

abs = absolute system
eff = effective
i = inner
id = ideal
o = outer
rel = relative system
s = static condition
t = total condition
V = vena contracta
0 = upstream of orifice
1 = downstream of orifice

References

[1] Zimmermann, H., Kutz, J., and Fischer, R., 1998, "Air System Correlations Part 2: Rotating Holes and Two Phase Flow," ASME Paper No. 98-GT-207.
[2] Dittmann, M., Dullenkopf, K., and Wittig, S., 2003, "Discharge Coefficients of Rotating Short Orifices With Radiused and Chamfered Inlets," ASME Paper No. GT2003-38314.
[3] Idris, A., and Pullen, K. R., 2005, "Correlations for the Discharge Coefficient of Rotating Orifices Based on the Incidence Angle," Proc. Inst. Mech. Eng., Part A, **219**, pp. 333–352.
[4] Dong, W., and Lienhard, J. H., 1986, "Contraction Coefficients of Borda Mouthpieces," ASME J. Fluids Eng., **180**, pp. 377–379.
[5] Parker, D. M., and Kercher, D. M., 1991, "An Enhanced Method to Compute the Compressible Discharge Coefficient of Thin and Long Orifices With Inlet Corner Radiusing," *Heat Transfer in Gas Turbine Engines*, ASME HTD Vol. 188.
[6] Maeng, D. J., Lee, J. S., Jakoby, R., Kim, S., and Wittig, S., 1999, "Characteristics of Discharge Coefficient in a Rotating Disk System," ASME J. Eng. Gas Turbines Power, **121**, pp. 663–669.
[7] Alexiou, A., Hills, N. J., Long, C. A., Turner, A. B., Wong, L.-S., and Millward, J. A., 2000, "Discharge Coefficients for Flow Through Holes Normal to a Rotating Shaft," Int. J. Heat Fluid Flow, **21**, pp. 701–709.
[8] von Karman, Th., 1921, "Über laminare und turbulente Reibung," Z. Angew. Math. Mech., **1**, pp. 233–252.
[9] Owen, J. M., and Rogers, R. H., 1989, *Flow and Heat Transfer in Rotating-Disc Systems*, Vol. 1, Rotor-Stator Systems, Research Studies Press Ltd., Taunton, Somerset, England.
[10] Idris, A., Pullen, K. R., and Read, R., 2004, "The Influence of Incidence Angle on the Discharge Coefficient for Rotating Radial Orifices," ASME Paper No. GT2004-53237.
[11] Bragg, S. L., 1960, "Effect of Compressibility on the Discharge Coefficient of Orifices and Convergent Nozzles," J. Mech. Eng. Sci., **2**(1), pp. 35–44.
[12] Reichert, A. W.,, Brillert, D., and Simon, H., 1997, "Loss Prediction for Rotating Passages in Secondary Air Systems," ASME Paper No. 97-GT-215.
[13] McGreehan, W. F., and Schotsch, M. J., 1988, "Flow Characteristics of Long Orifices With Rotation and Corner Radiusing," ASME J. Turbomach., **110**, pp. 213–217.
[14] Idris, A., Pullen, K., and Barnes, D., 2004, "An Investigation Into the Flow Within Inclined and Rotating Orifices and the Influence of Incidence Angle on the Discharge Coefficient," Proc. Inst. Mech. Eng., Part A, **218**, pp. 55–68.
[15] Lichtarowicz, A., Duggins, R. K., and Markland, E., 1965, "Discharge Coefficient for Incompressible Non-Cavitating Flow Through Long Orifices," J. Mech. Eng. Sci., **7**(2), pp. 210–219.
[16] Deckker, B. E. L., and Chang, U. F., 1965, "An Investigation of Steady Compressible Flow Through Thick Orifices," Proc. Inst. Mech. Eng., **180**, pp. 312–346.
[17] Hay, N., and Spencer, A., 1992, "Discharge Coefficients of Cooling Holes With Radiused and Chamfered Inlets," ASME J. Turbomach., **114**, pp. 701–706.
[18] Meyfarth, P. F., and Shine, A. J., 1965, "Experimental Study of Flow Through Moving Orifices," ASME J. Basic Eng., **87**, pp. 1082–1083.
[19] Rohde, J. E., Richards, H. T., and Metger, G. W., 1969, "Discharge Coefficients for Thick Plate Orifices With Approach Flow Perpendicular and Inclined to the Orifice Axis," NASA Technical Report No. TN D-5467.